MODELLING UNCONSOLIDATED RUBBLE FORCES ON A CYLINDRICAL STRUCTURE

R.F. McKenna and S.E. Bruneau and J.A. Guzzwell
C-CORE, Memorial University of Newfoundland
St. John's, NF, CANADA, A1B 3X5

ABSTRACT

Scale model experiments were conducted to address the interaction between a cylindrical structure and unconsolidated ice ridges. The tests were conducted with a 0.32 m diameter structure at speeds ranging between 0.02 m/s and 0.2 m/s. The ridges were constructed by piling broken ice rubble into 12 m long channels in level ice, producing ridges which were up to 3 m wide and 0.5 m deep. Full ridge keel profiles were obtained using an underwater acoustic profiler and piece size distributions of the ice blocks were determined using a video imaging technique. Except in the experiments at the slowest speed, local failure occurred during the initial penetration until a plug of ice blocks was pushed out of the back end of the ridge. The peak loads corresponded with the formation of this plug. The vertical shear planes of the plug tended to flare out at an angle of approximately 30° and there was more of a flare at the lower speeds. The portion of the ridge traversed at the time of maximum load varied between 20% for the slow speeds and 45% for the fastest ones. There was no apparent effect of interaction speed on the peak forces over the range tested.

INTRODUCTION

It has been speculated that the keels of first year ice ridges are significant contributors to the overall loads on cylindrical and conical structures. Large first year ridge loads have been measured against structures in Cook Inlet (Blenkarn, 1970) and on light piers in the Baltic Sea (Määttänen and Hoikkanen, 1990). As well, the piers for the Northumberland Strait bridge linking New Brunswick and Prince Edward Island (PEI) have been designed for considerable ridge keel loads. Similar concerns have been raised with regard to concepts for multi-leg offshore production structures.

Several recent efforts have focused on an improved understanding of the keel failure process and on the refinement of analytical models. The present experiments were conducted to assess the feasibility of using scale model tests in an ice tank to model first year ridges. Full details of these experiments in unconsolidated ridges are given in McKenna *et al.* (1995). The tests provide a means of correlating the forces with the failure process, including the coincidence of peak load and "plug" failure, and the ridge penetration at this event. To date, the influence of ice speed has not been resolved for ridge impacts on any structures and this was also considered.

The present effort was a pilot program which paved the way for subsequent experiments involving conical structures, much larger ridge keels and refrozen ridge cores. As a result, considerable effort went into the documentation of test conditions and failure processes. Ridges formed by piling ice from elsewhere in the tank into pre-cut channels were profiled using an acoustic system attached to a moving underwater carriage. Aside from the documentation of keel shape, these measurements provided confirmation of ridge porosity and ice density estimates. Above water and underwater rubble accumulations were documented and the ice block size distribution was determined using digital video image processing. A unique feature of the experiments was the clear evidence of "plug" failure from above water and underwater video.

EXPERIMENTAL SETUP

The tests were conducted in the ice tank at the Institute for Marine Dynamics in February 1995. The structure was a 0.32 m diameter aluminum cylinder mounted to a small movable carriage suspended beneath the load frame of the main ice tank carriage. Since the structure was designed to represent a full scale structure with a 10 m diameter, the nominal scale for the experiments was 1:32. Further details of the test rig, designed originally for a series of experiments on tanker mooring in pack ice, can be found in Spencer and Jones (1995). The structure was connected directly to a dynamometer which was then connected to the small carriage. Four load cells were placed in the horizontal plane, with two measuring lateral loads and two measuring the load along the direction of structure motion. Since the maximum expected ridge depth was approximately 0.5 m, the structure was lowered in the water such that the base was 0.6 m below the water level. The setup is illustrated in Fig. 1.

The loads were measured by an arrangement of four load cells, two

oriented to measure lateral forces (Y direction), and two oriented to measure forces in the longitudinal direction (X direction). Structure position and carriage speed data were logged at 10 Hz, while the load cell measurements were logged at 20 Hz. A 5 Hz Butterworth digital low-pass filter was applied to the data from each load cell before adding the data to obtain longitudinal and lateral forces.

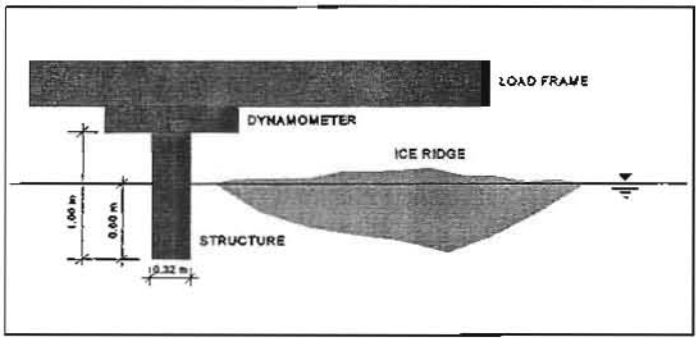

Fig. 1 Schematic of cylindrical structure

The friction coefficient between the ice and the structure surface was measured to be 0.13. This was based on direct measurements of sliding friction at 0.258 m/s on a 15 cm × 15 cm ice block for normal stresses of up to 13 kPa.

The experiments were documented using video cameras above and below the water surface. The above water cameras were positioned to the side and in front of the structure. The underwater cameras were located fore and aft at the tank centre line.

MODEL ICE RIDGES

The ridges were constructed from a model ice with ethylene glycol as the primary additive (for details, see Timco, 1986). During the freezing process, fine bubbles were introduced into the ice to achieve a realistic density (Spencer and Timco, 1990). At the time of ridge construction, the average density of blocks from the ice sheet was measured to be 882 kg/m^3 based on an immersion technique. Since the density of the water was 1002.5 kg/m^3, the ratio of ice to water density was 0.88. The actual density of blocks in the ridge was not measured at test time, which was approximately 6 hours later. From previous experience, the density of submerged blocks tended to increase asymptotically to 930 kg/m^3 within 24 hours, while that of elevated blocks decreased to approximately 750 kg/m^3 because of brine drainage.

The ice sheet thickness was 30 mm which, for a scale of 1:32, gives a full scale thickness of 0.96 m. The 30 mm thickness is an approximate lower limit on the level ice sheet thickness that can be grown in the tank and for which the properties can be controlled accurately. The constituent thickness of most ridges is of the order of 0.2 m to 0.5 m, so that the blocks tested are thicker at this scale. The present results can be interpreted at other scales, as long as allowance is made for proper scaling of the test speed and the rubble shear strength.

The full scale flexural strength of sea ice ranges from below 300 kPa to 700 kPa. The application of a scale factor of 1:32 yields a range of 10 kPa to 25 kPa. The flexural strength measured in the level ice decreased from 26 kPa to 10 kPa over the test period, so the model ice was quite realistic in this regard.

Two ridges, 2 m and 3 m in width, were constructed for the present tests. To build each ridge, two parallel saw cuts were first made in the level ice across the entire 12 m breadth of the tank. Ice from elsewhere in the tank was then lifted using the service carriage and dumped between the saw cuts. The 2 m wide ridge was constructed from 17 m of the level ice sheet and the 3 m wide ridge was made from 28 m of level ice.

RIDGE GEOMETRY

The underside of the ridges were measured using an acoustic profiler developed at C-CORE. Details of the system are documented in the Appendix. Six transducer/receiver pairs were mounted 0.40 m apart, 1.75 m below the water surface, on a video carriage which moved with the main carriage. The ridge profiles were obtained just prior to the commencement of the tests on each ridge. The profiler was stepped forward under the ridge by moving the main carriage in increments of 0.25 m for the 2 m wide ridge and 0.375 m for the 3 m wide ridge.

Above water profiles were obtained by measuring manually the distance from a fixed elevation on the service carriage to the water surface and to the ridge sail. These were measured every 0.25 m across the width of the ridges.

Because of the construction technique, the ridge profiles were approximately uniform across the tank. For the 2 m wide ridge, one above water profile and six underwater profiles were taken. For the 3 m wide ridge two above water and four underwater profiles were recorded. The ridge cross-section data are summarized in Table 2 and the profiles are plotted in Fig. 2 and 3. The thin lines document the individual profiles which were then averaged to obtain the thick lines.

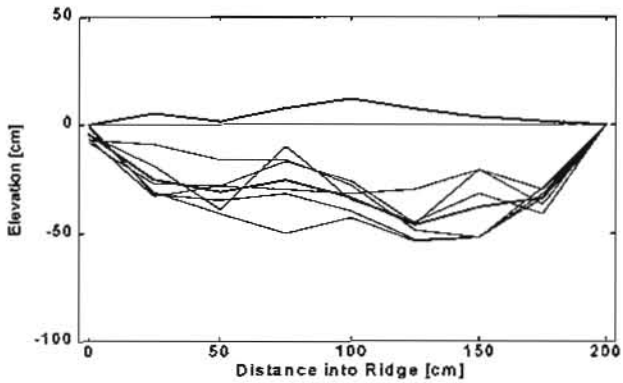

Fig. 2 Cross section of the 2 m wide ridge - the heavy line represents the average for all profiles

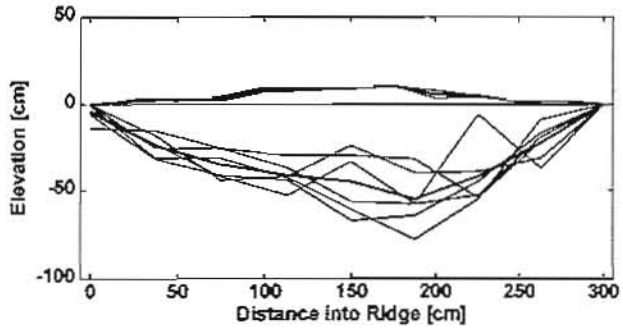

Fig. 3 Cross section of the 3 m wide ridge - the heavy line represents the average for all profiles

TABLE 1 Ridge properties and test matrix

RIDGE PROPERTIES	Run 1	Run 2	Run 3	Run 4	Run 5	Run 6
Ridge #	1	1	2	2	2	2
Ridge width (m)	2	2	3	3	3	3
Ridge sail x-section area (m^2)	0.1	0.1	0.15	0.15	0.15	0.15
Ridge keel x-section area (m^2)	0.59	0.59	1	1	1	1
Total ridge x-section area (m^2)	0.69	0.69	1.15	1.15	1.15	1.15
Ridge porosity	0.26	0.26	0.27	0.27	0.27	0.27
INTERACTION DATA						
Speed (m/s)	0.019	0.187	0.187	0.131	0.075	0.019
Ice/structure friction coef.	0.13	0.13	0.13	0.13	0.13	0.13
Structure diameter (m)	0.32	0.32	0.32	0.32	0.32	0.32
Logitudinal						
Peak longitudinal force (N)	332	331	852	592	692	541
Displacement to peak longit. (m)	0.342	0.595	1.336	1.177	1.05	0.681
Fraction of ridge to peak longit.	0.171	0.298	0.445	0.392	0.350	0.227
Lateral						
Peak lateral force (N)	68	73	121	177	171	347
Displacement to peak lat.. (m)	0.674	1.74	2.18	1.283	1.16	1.418
Fraction of ridge to peak lat.	0.337	0.870	0.727	0.428	0.387	0.473
Resultant						
Peak resultant force (N)	332	332	852	594	703	557
Displacement to peak res. (m)	0.342	0.595	1.336	1.203	1.05	1.272
Fraction of ridge to peak res.	0.171	0.298	0.445	0.401	0.350	0.424
VIDEO DATA						
Distance to plug (m)	0.38	0.81	1.17	1.1	1	0.64
Fraction of ridge to plug	0.19	0.41	0.39	0.37	0.33	0.21
Wedge flare angle (deg)	-	30	30	30	45	-
Max. wedge width (in diameters)	-	3 D	4 D	3-4 D	>5 D	
Surcharge height above water (cm)	13	12	20	21	21	12

Using the average above water and underwater profiles, estimates were made of the cross-section areas by numerical integration. These are reported for the two ridges in Table 1. If the porosities of the above and under water portions of the ridges are the same, then estimates of the ice density can be made. The density values shown in Table 1 are marginally lower than those calculated from the direct measurements of ice blocks described above. The agreement, however, is quite good considering the irregularity of the top and bottom surfaces of the ridges.

Estimates of the ridge porosity were made based on the measured ridge cross section areas, and on the length and thickness of the level ice used to build the ridges. The porosities were 0.26 for the 2 m wide ridge and 0.27 for the 3 m wide ridge, which are well within the range of field measurements.

The 2 m wide ridge was designed to be roughly triangular in cross section with a maximum depth of 0.5 m and an underwater slope of 33°. As seen in Fig. 2, the shape is probably more parabolic than triangular. The wider 3 m ridge was only marginally deeper and had a more gradual underwater slope as illustrated in Fig. 3. Although a trapezoidal section was intended, very little of the bottom surface could be considered flat.

ICE BLOCK GEOMETRY

Block dimensions were estimated from video images of the floating rubble following the tests. From a digitized video frame, the block length and width dimensions in the plane of the water surface were determined for 160 blocks. The third dimension in the vertical plane was assumed to be the initial ice sheet thickness of 3 cm. The statistics of these dimensions are shown in Table 2. The means of the length and width were 3.1 and 2.0 times the ice thickness. The smallest widths were approximately the 3 cm ice thickness and the largest length was between 8 and 9 times the ice thickness. On average, the ratio of the length to the width was 1.6.

TABLE 2 Summary of block size statistics based on a video image of floating rubble following tests of the 2 m wide ridge

Description	Mean (cm)	Standard Deviation (cm)
Ice Thickness	3.0	-
Length	9.2	2.7
Width	6.0	4.0
Length × Width	63.8	60.1
Length / Width	1.6	

A comparison can be made between the present results and those compiled by Veitch *et al.* (1991) for ridges in the Baltic Sea. The field data indicate that the length and the width were approximately 3 and 2 times the ice thickness, and that the ratio of maximum to minimum block dimension was 1.5. The comparisons between the field and laboratory data are remarkable considering the fact that no specific effort was made to control the block sizes in the ice tank.

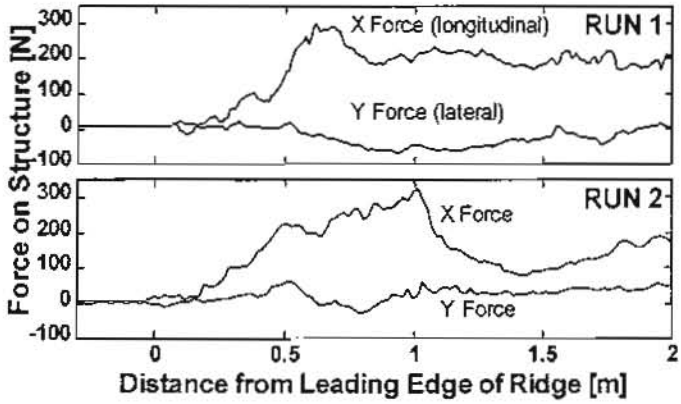

Fig. 4 Longitudinal and lateral forces as a function of penetration for Runs 1 and 2 through the 2 m wide ridge

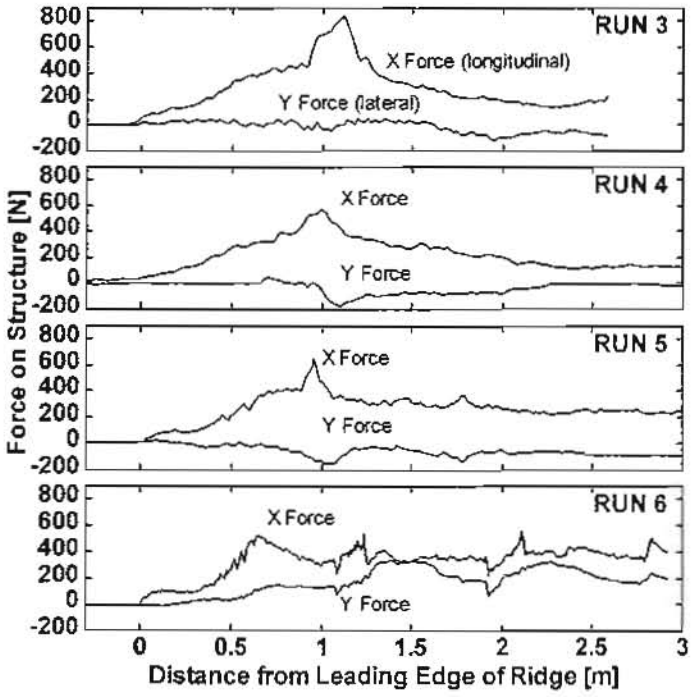

Fig. 5 Longitudinal and lateral forces as a function of penetration for Runs 3, 4, 5 and 6 through the 3 m wide ridge

TEST MATRIX

A total of six runs was made using a single ice sheet. As noted above, ridges with widths of 2 m and 3 m were built, simulating triangular and trapezoidal cross sections. Because the structure diameter was only 0.32 m, it was possible to make several parallel runs through each ridge at different speeds. The speed was varied between 0.019 m/s and 0.187 m/s as shown in Table 1.

FORCE - DISPLACEMENT RELATIONS

The reduced force-displacement traces for the six tests are shown in Fig. 4 and 5. Both longitudinal (upper curve) and lateral (lower curve) forces are plotted against relative displacement. The origin of the relative displacement is the position of the leading edge of each ridge as determined by synchronising data files with the video records.

The peak longitudinal, lateral and resultant forces on the structure and the position (within the ridge) at which they occurred are documented in Table 1. The peak longitudinal forces are shown to be between three and five times the peak lateral forces. The peak lateral forces occurred at nearly double the penetration of the longitudinal peaks. The longitudinal force is shown plotted against the lateral force for all tests in Fig. 6. The forces were resampled at a displacement increment of 1 cm and have been normalized with respect to the peak longitudinal value. For all runs, the lateral force never exceeded 0.3 times the maximum longitudinal force and there was some correlation between the largest lateral forces and the largest longitudinal forces. The data points for the slowest structure speed (runs 1 and 6), identified in Fig. 6, resulted in the largest lateral forces. From the video records, the high lateral forces occurred when the ridge failed as a beam which was then pushed back into the supporting level ice.

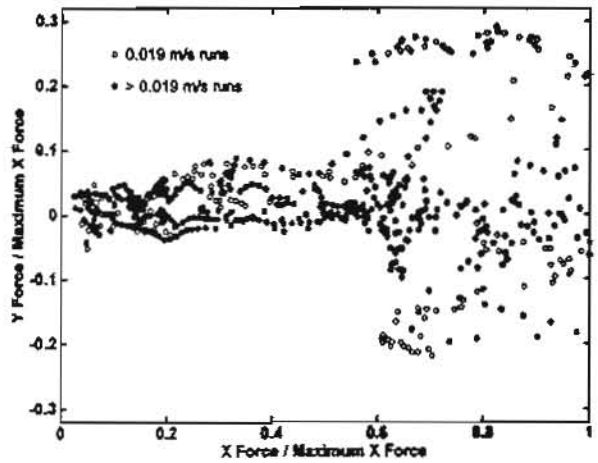

Fig. 6 Longitudinal vs lateral forces for all runs normalized with respect to the peak longitudinal force in each run

EFFECT OF RIDGE DIMENSIONS AND TEST SPEED

The peak longitudinal load increased significantly for the 3 m wide ridge when compared to the 2 m wide ridge. This relation is shown as a function of ridge cross section area in Fig. 7. Averaged over the different test speeds, the load more than doubled for the wider ridge while the ratio of cross section areas was 1.7. Since the ridges were geometrically similar, it is doubtful whether cross section area alone can be used to determine ridge loads on cylindrical structures.

Coincidentally, the peak longitudinal and lateral forces for the 2 m ridge were consistent at the two speeds tested so as to be nearly indistinguishable. Based on the data shown in Fig. 8, the peak loads were relatively insensitive to velocity.

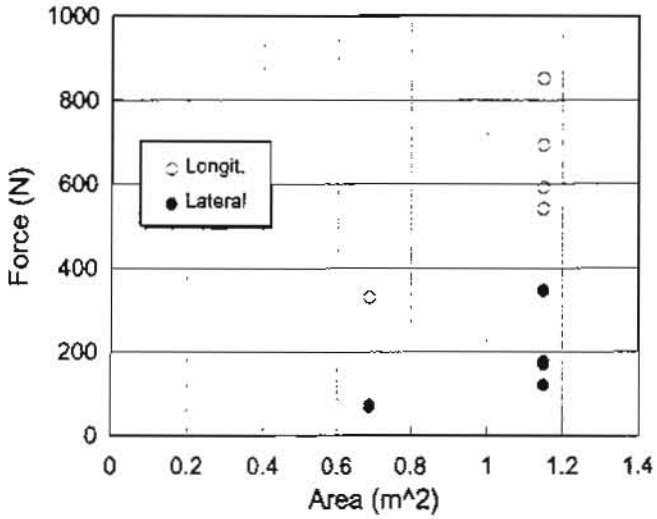

Fig. 7 The influence of ridge cross-section area on the peak longitudinal and lateral forces

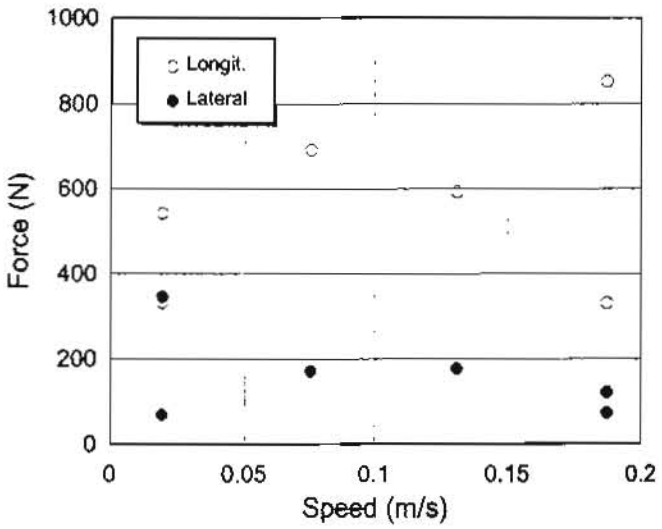

Fig. 8 The influence of speed on the peak longitudinal and peak lateral forces

FAILURE MECHANISMS

While the forces may not have been influenced by test speed, there did appear to be a change in the failure mode. For the slowest speed, observations from the video record indicated that both ridges failed horizontally as beams with a hinge crack at the structure. On the other hand, ridge failure was characterized by local ice block movement preceding the formation of a wedge-like plug at the higher speeds. The plug geometry is shown in Fig. 9. From Table 1, an increased penetration into the ridge before plug failure was observed for those experiments exhibiting the plug-like failure.

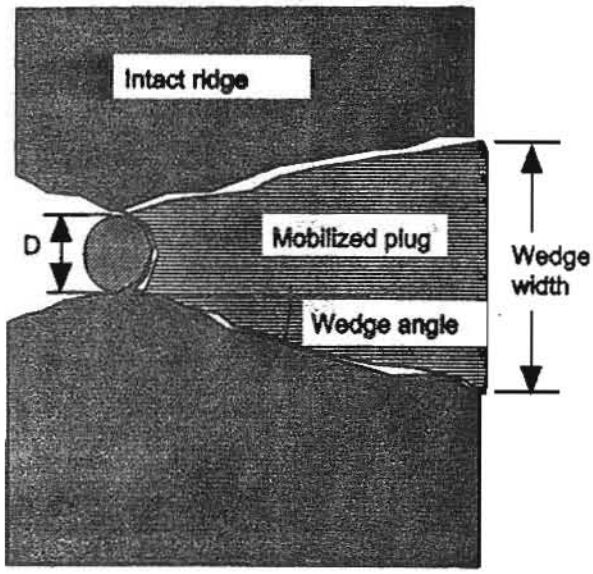

Fig. 9 Schematic of plug failure mechanism

Table 1 also summarizes some of the observations based on the four synchronous video records. A direct correlation between the point at which the plug was first observed and the peak longitudinal load can be seen in the tabulated data. Allowing for errors in the observations of plug formation, the two appear to be coincident. It was also apparent that the shape and size of the plug varied with indentation rate. Generally, more rubble was displaced at lower rates than at higher rates. The plug, comprised of a large mass of rubble leading the advancing structure, eventually rolled off to one side or the other resulting in the apparent delay and arbitrary sign of the lateral forces.

The plugs formed in the highest speed tests (Runs 2 and 3, 0.187 m/s) had flare angles of approximately 30° outward from the direction of structure advance. Typically, the wedges flared out from the full width of the structure to a maximum width which is indicated in Table 5 in terms of the structure diameter. The sizes of the plugs for Runs 4 and 5 (3 m ridge, 0.131 m/s and 0.075 m/s) were larger than for Runs 2 and 3. For Runs 1 and 6 (0.019 m/s), no obvious plug failure took place. For Run 1, the ridge failed in horizontal bending with a central crack in front of the structure and hinge cracks on the side. For Run 6, a large piece of the ridge was displaced and pushed into the supporting ice sheet.

In summary, the plug failure process can be characterized from the video record as follows:

- progressive compression led to full activation of the plug;
- rubble accumulation remained static after the plug was activated;
- blocks within the plug had no relative movement and the plug maintained steep, rough sides;
- a shear surface bounded the moving rubble mass and there was little or no continuum of motion; and
- the plug flared outward at an angle of approximately 30°.

Rubble accumulation had an influence on the forces imparted to the structure. The pile-up of rubble above the water surface was clearly documented by the side video camera and the surcharge at this point is given in Table 1. It was derived by digitizing one video image prior to

the entry of the structure into the ridge and one at the time of plug formation. The surcharge height above the water surface was obtained from the total height of the structure above the water surface, less the distance from the top of the structure to the top of the rubble. The pier diameter was used for scaling pixel values.

For the 2 m ridge (Runs 1 and 2), rubble height at plug failure was 12 cm to 13 cm so there was no noticeable speed effect. In this case, the rubble height was approximately the same as the sail height at the centre of the ridge. For Runs 3, 4 and 5 (3 m ridge), the rubble height against the structure was about 20 cm which is significantly in excess of the maximum sail height. In Run 6, the ridge failed at a smaller penetration and the surcharge was only 12 cm.

The video camera angles did not permit an accurate estimate of underwater surcharge; however, it appeared that the build-up was substantially less than above the water surface.

DISCUSSION

An estimate can be made of the stress on the failure planes at the point of plug failure for runs 2 through 5. The average failure stress on the two planes for the 2 m wide ridge was approximately 0.34 kPa, while it was 0.78 kPa for the 3 m wide ridge. If the rubble behaved as a frictional material in which shear strength increased with ice depth, this could help to explain the difference.

No independent measurements of the shear properties of the model ice rubble were made for the present tests. Rubble shear properties have been measured in IMD's ice tank using a shear box apparatus with floating model ice rubble by (Case, 1991a,b), and *in situ* ridge measurements were made using vertical punch (McKenna *et al.*, 1996) and direct shear (Bruneau *et al.*, 1996) techniques. For confining pressures of 1 kPa, maximum shear stresses reached just over 1 kPa. The maximum shear stress measured for ridge keels in the Baltic Sea was 4 kPa for a 3.9 m deep ridge (Leppäranta and Hakala, 1992).

The lack of comprehensive field data makes it difficult to scale the results of the present experiments. The authors are involved in a couple of field experiments to measure ice rubble properties this winter and the results of these should assist with the estimation of loads on fixed structures.

CONCLUSIONS

The present experiments address some of the issues involved in the failure of first year ice ridges against a cylindrical structure. At the higher speeds, the peak load was governed by a plug failure mechanism while beam failure of the ridge dominated at the lowest speed. The vertical shear planes of the plug tended to flare out at an angle of approximately 30° and there appeared to be more of a flare at the lower speeds. The portion of the ridge traversed at maximum load increased with the speed of the interaction..

In spite of the different failure mechanism at the slowest speed, there was no discernible influence of test speed on the maximum longitudinal force. Averaged over all speeds, the peak load for interaction with the 3 m wide ridge was more than double that for the 2 m wide ridge while the cross section area was only 1.7 times greater. As long as plug failure occurred, the lateral forces did not exceed 30% of the longitudinal values.

ACKNOWLEDGEMENTS

Funding for the project was provided by the National Energy Board and the Panel on Energy Research and Development. The test series was conducted while Richard McKenna was employed at the Institute for Marine Dynamics (IMD) of the National Research Council of Canada. Brian Hill and Craig Kirby of the IMD were responsible for all instrumentation and the operation of the tank. Don Spencer (formerly of the IMD, now with Marineering Ltd.) developed the structure and carriage setup and also assisted with data analysis procedures. The underwater profiler design, setup and data processing were performed by Patricia LeFeuvre and Fabian Hartery of C-CORE.

REFERENCES

Blenkarn, K.A. (1970) Measurement and analysis of ice forces on Cook Inlet structures, OTC paper 1261, Offshore Technology Conference, Dallas, Texas, vol. II, pp.365-378.

Bruneau, S.E., McKenna, R.F., Croasdale, K.R., Crocker, G.B. and King, A.D. (1996) *In situ* direct shear of ice rubble in first year ridge keels, in Proceedings of the 49th Canadian Geotechnical Conference, St. John's, Newfoundland, Vol.1, pp.269-278.

Case, P.C. (1991a) A model scale study of the frictional and cohesive properties of floating ice rubble, Institute for Marine Dynamics Report LM-1991-03, 113p.

Case, P.C. (1991b) A continued study of the frictional and cohesive-like behaviour of floating model ice rubble, Institute for Marine Dynamics Report LM-1991-27, 25p.

Leppäranta, M. and Hakala, R. (1992) The structure and strength of first-year ridges in the Baltic Sea, Cold Regions Science and Technology. Vol. 20, pp.295-311.

Määttänen, M. and Hoikkanen, J. (1990) The effect of ice pile-up on the ice force of a conical structure, in Proceedings of the 10th IAHR Ice Symposium, Espoo, Finland, pp.1010-1021.

McKenna, R.F., Bruneau, S.E., Guzzwell, J., Hill, B. and Kirby, C.S. (1995) Pilot experiments with a cylindrical structure in unconsolidated ridges, Contract report prepared for the National Energy Board, NRC/IMD Report TR-1995-20, 32p.

McKenna, R.F., Bruneau, S.E. and Williams, F.M. (1996) *In situ* shear strength measurements of model ice rubble using a punch technique, in Proceedings of the 49th Canadian Geotechnical Conference, St. John's, Newfoundland, Vol.1, pp.279-286.

Spencer, D.A. and Jones, S.J. (1995) Experimental investigation into the response of a moored tanker to changes in ice drift angle, IMD Report TR-1995-16 (protected) prepared for CANMAR, 19p.

Spencer, D.S. and Timco, G.W. (1990) CD model ice - a process to produce correct density model ice, in Proc. of IAHR Ice Symposium, Espoo, Finland, pp.745-755.

Timco, G.W. (1986) EG/AD/S: a new type of model ice for refrigerated towing tanks, Cold Regions Science and Technology, Vol.12, pp.175-195.

Veitch, B., Lensu, M., Riska, K., Kosloff, P., Keiley, P. and Kujala, P. (1991) Field observations of ridges in the northern Baltic Sea, in Proceedings of the 11th International Conference on Port and Ocean Engineering under Arctic Conditions, St. John's, Canada, Vol.1, pp.381-400.

APPENDIX: ACOUSTIC PROFILER

The acoustic profiler consisted of six transducer/hydrophone pairs (mounted to the underwater video carriage which moved with the main carriage), an underwater box containing signal conditioning and multiplexing hardware, a customized 'chirp' circuit board, a multichannel waveform recorder and a personal computer. The system is illustrated

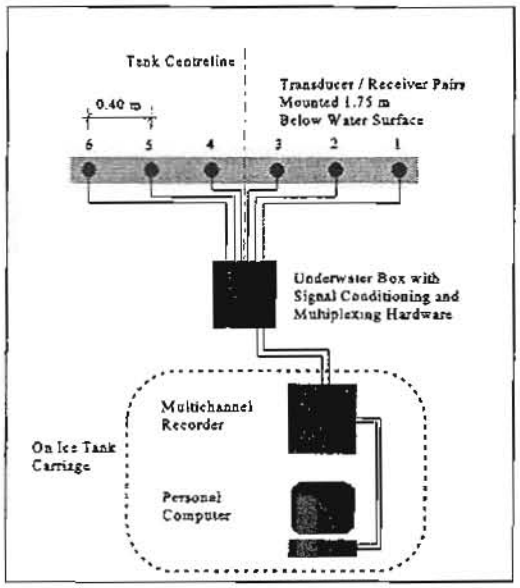

Fig. A1 Acoustic profiler layout

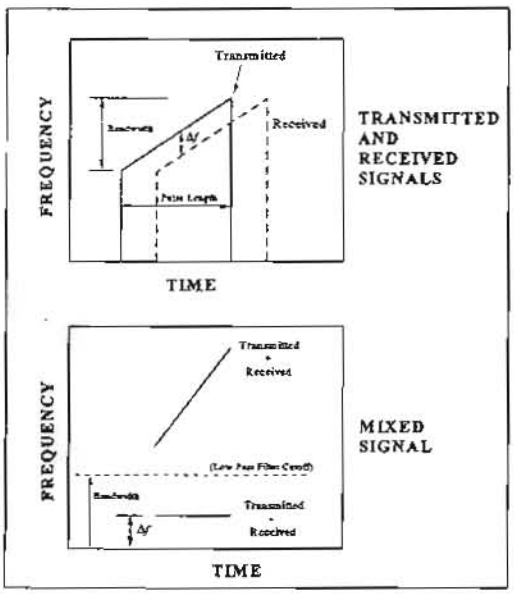

Fig. A2 Mixing of sent and received 'chirp' signals

in Fig. A1.

Frequency Modulated Continuous Wave (FMCW) or 'chirp' waveforms are commonly used in radar applications because they achieve high resolution and long ranges using recognizable signals with high energy and low peak power. The 'chirp' signal used for the profiler consisted of a sine wave with a linearly increasing frequency from 120 kHz to 160 kHz (bandwidth f_{bw} = 40 kHz) for a duration or pulse length of L_p. The 'chirp' signal was transmitted by one of a pair of transducers, then received by the other after reflection off the water surface or the ice blocks in the ridge keel. The received signal was multiplied or mixed with the transmitted signal as transmission took place. When the transmitted and received signals overlap, the mixed signal is made up of essentially two trigonometric functions with frequencies equal to the sum and difference of the frequencies of the two separate signals. This is shown by the following trigonometric identity

$$\cos A \cos B = \frac{1}{2}[\cos(A-B) + \cos(A+B)] \qquad \text{(A1)}$$

The component of the signal with the summed frequency $\cos(A+B)$ is filtered out of the resultant mixed signal with a low pass filter. The remaining frequency component, $\Delta f = (A-B)/2\pi$, is proportional to the time difference Δt between the transmitted signal and the received signal, and is proportional to the distance to the target. The whole process is illustrated in Fig. A2.

The low frequency signal was digitized and an FFT was performed in post-processing to extract the frequency Δf. The distance to the target was calculated using

$$\text{distance} = c\frac{\Delta t}{2} = c\frac{\Delta f L_p}{2 f_{bw}} \qquad \text{(A2)}$$

where c is the speed of sound in the ethylene glycol solution (approximately 1400 m/s at 0.1 °C). According to classical theory, the resolution of the system is $c/(2f_{bw})$ or approximately 2 cm. When high signal to noise ratios are achieved and conventional signal processing techniques are used, the actual resolution is significantly better than this. A transducer beam width of 10° meant that the footprint on the undersurface of the ice was about 25 cm.

Just prior to the experiment, the distance to the water surface was recorded for each of the six transmitter/receiver pairs and these values were used as reference data to determine the depth of the submerged ice ridge above each transducer pair. The keel depth of the ridge was calculated as $d_{water} - d_{ice}$, where d_{water} is the calibrated distance measured from the transducer pair to water surface and d_{ice} is the calibrated distance from transducer pair to the base of the ridge keel. Details are shown in Fig. A3.

The acoustic profiler described in this paper was an experimental model which was adapted for measuring ridge keels. Subsequently, a new profiler (the Digital Acoustic Radar Transceiver) was developed at C-CORE for the IMD ice tank. It includes all digital circuitry and the processing has been automated such that ridge or rubble profiles can be produced within minutes of the data acquisition.

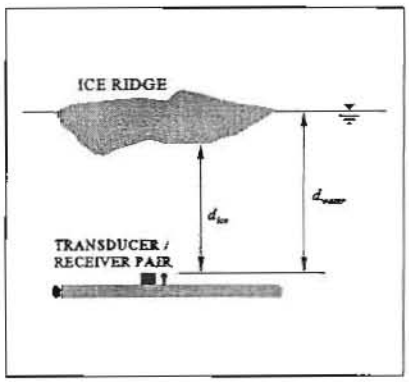

Fig. A3 Ridge depth measurements using acoustic profiler